

Optimising a balloon-borne polarimeter in the hard X-ray domain: from the PoGOLite Pathfinder to PoGO+

M. Chauvin^{a,b,*}, M. Jackson^{a,b}, T. Kawano^c, M. Kiss^{a,b}, M. Kole^{a,b,e}, V. Mikhalev^{a,b}, E. Moretti^{a,b,d}, H. Takahashi^c, M. Pearce^{a,b}

^a*KTH Royal Institute of Technology, Department of Physics, 106 91 Stockholm, Sweden*

^b*The Oskar Klein Centre for Cosmoparticle Physics, AlbaNova University Centre, 106 91 Stockholm, Sweden*

^c*Hiroshima University, Department of Physical Science, Hiroshima 739-8526, Japan*

^d*Max Planck Institut for Physics, D-80805 Munich, Germany*

^e*University of Geneva, CH-1211 Geneva, Switzerland*

Abstract

PoGOLite is a balloon-borne hard X-ray polarimeter dedicated to the study of point sources. Compton scattered events are registered using an array of plastic scintillator units to determine the polarisation of incident X-rays in the energy range 20 - 240 keV. In 2013, a near circumpolar balloon flight of 14 days duration was completed after launch from ESRANGE, Sweden, resulting in a measurement of the linear polarisation of the Crab emission. Building on the experience gained from this Pathfinder flight, the polarimeter is being modified to improve performance for a second flight in 2016. Such optimisations, based on Geant4 Monte Carlo simulations, take into account the source characteristics, the instrument response and the background environment which is dominated by atmospheric neutrons. This paper describes the optimisation of the polarimeter and details the associated increase in performance. The resulting design, PoGO+, is expected to improve the Minimum Detectable Polarisation (MDP) for the Crab from 19.8% to 11.1% for a 5 day flight. Assuming the same Crab polarisation fraction as measured during the 2013 flight, this improvement in MDP will allow a 5σ constrained result. It will also allow the study of the nebula emission only (Crab off-pulse) and Cygnus X-1 if in the hard state.

Keywords: X-ray, Polarimeter, Balloon, Crab, Simulation, Geant4

1. Introduction

Measuring the linear polarisation of X-ray emissions from astrophysical sources gives unique insight into the emission mechanisms at work and the geometry of the emitting region [1, 2]. Due to the difficulties in making sensitive measurements in this energy domain, only a few instruments have been able to successfully detect polarisation [3, 4, 5, 6]. The delicate control of systematic effects benefits from instruments specifically designed for polarimetric measurements.

PoGOLite is a purpose-built polarimeter working in the energy range 20 - 240 keV. It determines the linear polarisation of hard X-ray emission

from point sources by measuring the distribution of Compton scattering angles in a plastic scintillator detector array. The PoGOLite Pathfinder mission was designed to validate the instrument concept. Launched from the ESRANGE Space Centre at 08:18 UT on July 12th 2013, the payload was airborne for 14 days, making an almost complete circumpolar flight around the North Pole (average latitude of 68°). The prominent Crab X-ray source was observed for 14 hours. Data from this first flight revealed limitations of the design and a challenging background environment dominated by atmospheric neutrons. Based on the accumulated experience, a new design that will significantly improve the polarimeter performance is proposed.

After describing the instrument and its numerical simulation, the different modifications are presented along with their associated increase in po-

*Corresponding author

Email address: chauvin@kth.se (M. Chauvin)

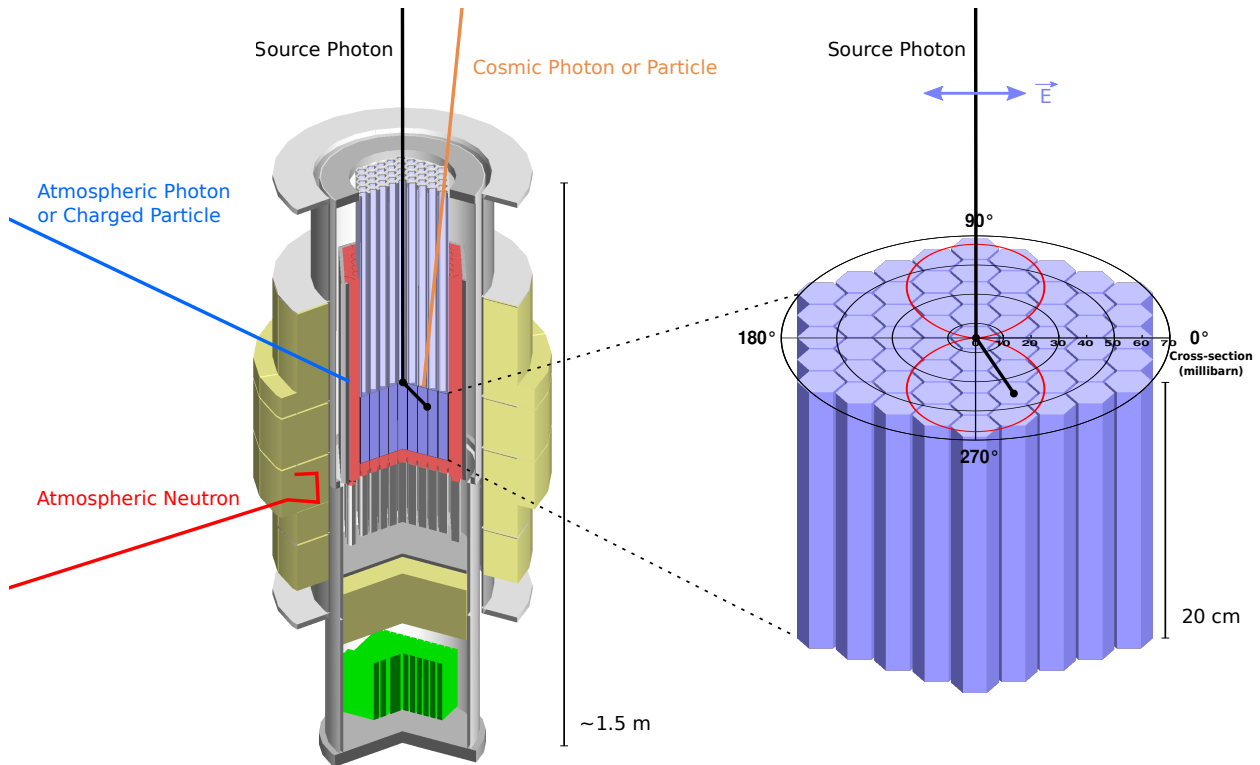


Figure 1: PoGOLite Pathfinder schematic view and detection principle. Left: the detector made of plastic scintillators (blue), the BGO anti-coincidence (red), the active plastic scintillator collimators (light blue), the photomultiplier tubes (grey) and the electronic components (green) are enclosed in a cylindrical housing. This inner housing is rotated around the viewing axis in order to remove systematic effects in the measurements. The detectors are surrounded by a passive shield made of polyethylene (yellow) to reduce the neutron background. The background components and their interactions in the instrument are represented by different coloured lines. Right: close-up view of the detector assembly. The 61 plastic scintillator rods, about 3 cm wide and 20 cm long, are closely packed to provide the azimuthal angle between two consecutive interactions (black dots). The Compton cross-section is overlaid on top (not to scale) to show the preferential scattering direction of the incoming polarised photons.

larimetric performance in terms of Minimum Detectable Polarisation (MDP) [7].

In the final section of the next design, PoGO+, is discussed for the Crab and Cygnus X-1 during the next balloon flight, planned for the summer of 2016.

2. The PoGOLite instrument

PoGOLite is a polarimeter making use of Compton scattering kinematics. When polarised photons undergo Compton scattering they have higher probability to scatter perpendicular to their polarisation vector. This is described by the Klein-Nishina differential cross-section:

$$\frac{d\sigma}{d\Omega} = \frac{1}{2} r_0^2 \epsilon^2 [\epsilon + \epsilon^{-1} - \sin^2 \theta \cos^2 \phi] \quad (1)$$

where r_0 is the classical electron radius, ϵ is the ratio between the scattered and incident photon energies, θ is the polar scattering angle and ϕ is the azimuthal scattering angle defined as the angle to the electric field vector. Within a polarimeter, this anisotropic process causes a modulation in the detected azimuthal angles and measuring the phase and amplitude of this modulation allows the polarisation angle and polarisation fraction of the source flux to be determined.

The PoGOLite Pathfinder uses an array of 61 plastic scintillator rods, giving an exposed detector area of 298 cm², and providing a high cross-section for scattering X-ray photons. The hexagonal rods are closely-packed to provide the azimuthal scattering angle of a photon interacting twice in the detector. Following the detection of an energy de-

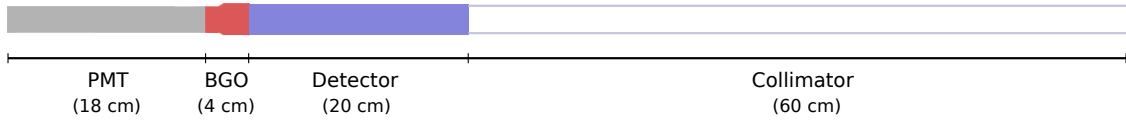


Figure 2: Sketch of a PoGOLite Pathfinder detector unit. The main detector (blue) is sandwiched between a BGO crystal (red) and a hollow 2 mm thick active collimator made of plastic scintillator (light blue). The three scintillators are read-out by the same PMT (grey) and their signals are identified by their different waveform shape.

posit above ~ 20 keV in one detector cell (assumed to be a photoelectric absorption event), the remaining cells are checked for a coincident lower energy deposit above ~ 0.5 keV (assumed to be a Compton scattering event). Each detector cell has a dynamic range of 20 - 120 keV. Since two-hit events are used for the polarisation analysis, the maximum (theoretical) energy range of the instrument becomes 20 - 240 keV. The polarimeter and detection concept are illustrated in Figure 1.

A detector rod (20 cm long) is sandwiched between two anti-coincidence components: a BGO scintillator (4 cm long) and an active collimator (60 cm long) made of plastic scintillator (see Figure 2). The three stacked scintillators are read out by the same photomultiplier tube (PMT) - based on the Hamamatsu R7899 design but modified to reduce the dark current. The sandwiched detector has a faster rise time to allow event discrimination based on the pulse shape. The anti-coincidence is complemented by 30 rods of BGO scintillators (60 cm tall) placed around the main detector cells. PMT signals are fed to charge-sensitive amplifiers, the outputs of which are sampled with 12 bit precision by flash analog-to-digital converters (ADC) operating at 37.5 MHz. Candidate polarisation events are identified through recorded energy deposits. An initial rejection of background events occurs using ADC waveform information and signals from the BGO veto system. The remaining waveform data is saved for post-flight analysis. The assembly housing the detector and anti-coincidence system is rotated during observations to eliminate possible systematic effects, e.g. due to differences in response between detector cells, as well as to provide a continuous distribution of scattering angles. A passive neutron shield made of polyethylene additionally surrounds the instrument. A detailed description of the instrument and data acquisition system can be found in [8].

3. The PoGOLite simulation

The PoGOLite simulation allows the performance of the polarimeter to be studied, depending on the observation environment and detector configuration. The simulation is divided in two parts (see Figure 3). The first part simulates particle interactions in the instrument and includes source emission (e.g. Crab) and background processes (neutrons and photons). The second part reproduces the instrument response (scintillator light-yield, PMT behaviour and data acquisition system).

The first part of the simulation has been developed using Geant4 [9] 10.0 patch-02 and includes the instrument mass model (Figure 1). As Geant4 is designed to simulate static geometries, a custom function has been developed to allow the rotation of the polarimeter. Particles are generated according to source and background emission models including air density depending on the instrument altitude and source elevation. The particle interactions are simulated using appropriate standard physics lists, G4EmLivermorePolarizedPhysics for photons and QGSP_BERT_HP for neutrons. The energy and position of each interaction is stored in a ROOT [10] tree format.

The second part of the simulation reproduces the conversion of energy deposits into ADC values and emulates the data acquisition system of PoGOLite. Every interaction is converted into scintillation light, then into a PMT signal [11]. The different scintillator material properties, their light-yield non-linearity (quenching), the scintillation light attenuation, the production of photoelectrons, the multiplication of charges and the conversion into ADC values (digitisation) are all accounted for. Every detector cell is independently treated using measured calibration parameters such as the conversion from energy to number of photoelectrons relation (scintillator-dependent) and the single photo-electron peak position in ADC values (PMT-dependent). Unintentional optical cross-talk

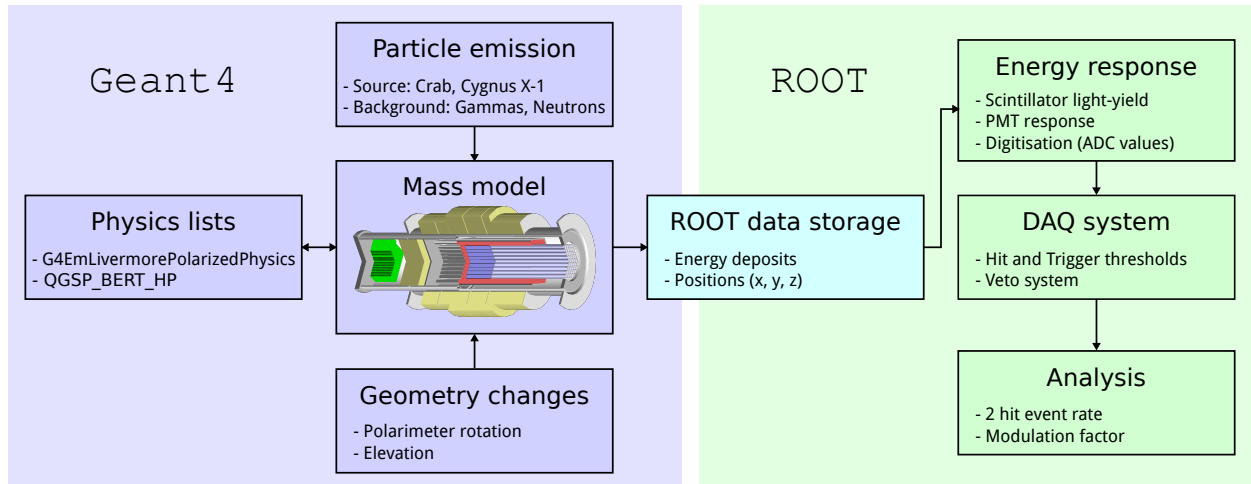


Figure 3: PoGOLite simulation flow-chart. The simulation is divided in two main parts, one simulating the particle interactions (using the Geant4 toolkit, blue) and one reproducing the instrument response (using the ROOT environment, green).

between detector cells (discovered after the 2013 flight) is also taken into account based on laboratory measurements performed with a pulsed blue LED. Once deposited energies from Geant4 are converted into ADC values, event selection criteria imposed by the data acquisition system of PoGOLite are applied. First, every detector cell yielding a PMT signal amplitude less than 10 ADC values is ignored (zero-suppression hit threshold). Then a trigger is issued if one of the signal amplitude exceeds 300 ADC values. After applying these thresholds, the veto system rejects the event if there is any signal in the anti-coincidence system or if any energy deposit exceeds an upper discriminator threshold (i.e. likely corresponding to a cosmic ray interaction). For interactions in any one of the 30 BGO units that surround the main detector, the event is discarded if above the hit threshold. For the active collimators and the BGO scintillators placed above and below the detector respectively, the discrimination is based on the waveform shape. Using laboratory measurements made on single scintillator elements separately coupled to a PMT, analytical functions have been established linking the energy deposit to the waveform amplitude after two typical rise times called “fast output” (~ 107 ns) and “slow output” (~ 400 ns). These functions allow the veto system based on waveform discrimination to be implemented in the simulation using the same algorithm as on-board PoGOLite. Only events that pass the veto with two interactions in different detector cells are considered as polarisa-

tion events. The azimuthal angle is determined and filled in a histogram resulting in a sinusoidal modulation curve from which the polarisation angle (phase) and polarisation fraction (amplitude) are extracted.

The simulation has been developed and validated using data taken during the preflight calibration of the polarimeter [12]. The modulation factor for a 100% polarised source (M_{100}) of 53.3 keV photons has been found to be $(21.3 \pm 0.9)\%$ from measurement and $(23.7 \pm 0.14)\%$ from simulation. These simulation results were based on a simplified implementation of the veto system, which assumed that discrimination between a waveform from the detector and one from the anti-coincidence was not possible below 100 ADC values (5 keV). After updating the simulation with a more realistic implementation of the veto system as described above, M_{100} is $(22.97 \pm 0.22)\%$, which is compatible with measurements within 1.5 standard deviations.

Waveform discrimination for the 2013 flight data was found to be more challenging than for the preflight calibrations. There are two reasons for this. Firstly, the variable temperature environment during the flight affect the waveform pedestal level so a temperature correction needed to be applied. Secondly, many waveforms with a shape corresponding to a mix of “slow” rise-time from the collimator and “fast” rise-time from the detector were found in the data. These super-imposed waveforms, coming from simultaneous energy deposits in a collimator and a detector of the same unit (e.g. via Comp-

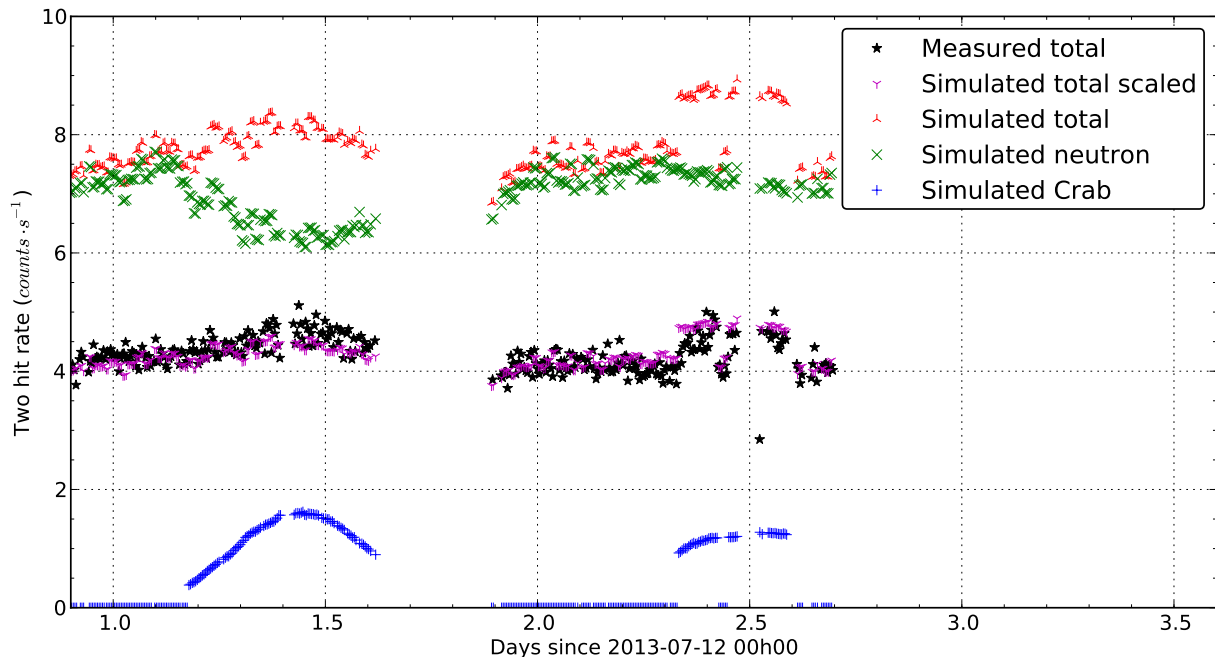


Figure 4: PoGOLite Pathfinder two hit (polarisation event) rate during the 2013 flight. Measured rate is shown (black stars) with the simulated rates; Crab (blue pluses), neutron (green crosses), total (red tripods up) and scaled total (purple tripods down). The total includes the Crab, the neutron and the photon background rates. The latter is not shown and contributes as a constant $0.28 \text{ counts}\cdot\text{s}^{-1}$. The simulation is scaled down to account for the waveform selection efficiency of the instrument data. The gaps in the data correspond to intervals where the data acquisition was not running.

ton scattering), are very similar to waveforms from the detector only, making them difficult to reject. As a consequence, the post-flight event identification using only two variables for waveform discrimination (the “fast output” and the “slow output”) showed poor efficiency, resulting in a low signal-to-background ratio.

In order to improve the veto efficiency, a new discrimination technique using a principal component analysis (PCA) was developed and used on the flight data [8]. This method, making use of more information from the waveform shape (ten variables instead of two), reduces the total number of accepted two-hit events (from 8.4 to 4.6 Hz) but significantly increases the signal-to-background ratio (from 1:7 to 1:4). Figure 4 shows the two-hit polarisation event count rate observed during the 2013 flight, showing a clear increase during the two Crab observations. The simulated Crab rate, simulated neutron rate and simulated total rate are also shown. The photon background, composed of the cosmic X-ray background, secondary atmospheric photons and the 511 keV line, is included in the

total but is not shown as it contributes to only $0.28 \text{ counts}\cdot\text{s}^{-1}$ and is assumed to be constant. The simulated Crab rate takes into account the altitude and pointing elevation of the polarimeter. The neutron rate is simulated using the model presented in [13] and takes into account the directionality of the incident neutron flux, variations in altitude and magnetic latitude of the instrument as well as the solar activity at the time of the measurement. The reduction in neutron rate around 1.15 days, as shown in Figure 4, is confirmed by a dedicated on-board neutron detector and coincides precisely with a decrease in the neutron flux measured by the Oulu Neutron Monitor¹. Additional details regarding the flight are presented in [8]. The simulated total rate is then scaled down to account for the PCA waveform selection efficiency. In the next sections, this scaling is applied to the simulations to be representative of the actual data analysis.

¹On-ground cosmic ray station, <http://cosmicrays.oulu.fi/>.

4. New design: PoGO+

A wealth of improvements to the PoGOLite Pathfinder polarimeter design have been identified based on the analysis of the 2013 flight data. This section reports on the performance study of different configurations to optimise the polarimeter for the next flight. These studies, made using the PoGOLite simulation, are presented in an incremental (cumulative) way to show the overall increase in performance. The incremental design changes are likely not independent and therefore have no realistic interpretation when treated separately. To be representative of a real flight, the Crab simulations assume the average column density as experienced during the 2013 flight, and the neutron background simulations assume the average neutron activity that occurred during the flight (based on the model from [13]). The Minimum Detectable Polarisation at 99% confidence level (MDP) is used as a figure of merit to compare the different configurations. It is defined as:

$$\text{MDP} = \frac{4.29}{M_{100}R_S} \sqrt{\frac{R_S + R_B}{T}} \quad (2)$$

where R_S is the source rate, R_B the background rate and T the observation time. For all following studies, the observation time is set to 6 hours (daily Crab observation window).

4.1. Scintillator coating

The relatively low M_{100} of the PoGOLite Pathfinder has been found to be due to unintentional leakage of scintillation light between detector cells. A one-hit event causing a leakage can incorrectly be tagged as a two-hit polarisation event ("false positive") and a two-hit polarisation event with leakage can erroneously be rejected as having higher multiplicity ("false negative"). Although the fraction of light leaking into other detector units is small ($\sim 1\%$), it significantly degrades the polarimeter performance reducing the M_{100} by $\sim 27\%$ (relative). Figure 5 shows the improvement in terms of MDP when the optical cross-talk is suppressed. This is achieved by changing the wrapping of the detector cells, using opaque DuPont Tedlar sheets and black heat-shrink material. The light collection can also be improved which directly impacts the polarimeter performance by decreasing the lower limit of the energy range and increasing the M_{100} . This is of crucial importance for Compton polarimeters such as PoGOLite, where

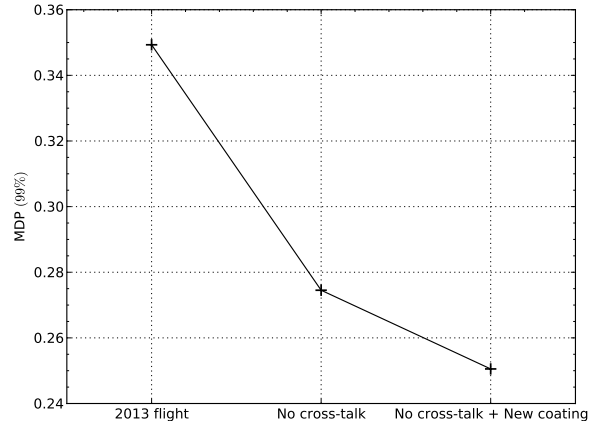


Figure 5: Polarimeter performance in terms of MDP for three configurations. The left-most point corresponds to the original design that was launched in 2013, the centre point to the suppression of optical cross-talk and the right-most point to additionally changing the reflective coating of the detector cells.

low energy deposits must be clearly distinguishable², since the Crab has an emission spectrum $\sim 9.7(E/\text{keV})^{-2.1} \text{ photons} \cdot \text{cm}^{-2} \cdot \text{s}^{-1} \cdot \text{keV}^{-1}$. By changing the reflective coating using white PTFE tape instead of BaSO₄-loaded epoxy and 3M ESR Vikuiti instead of 3M VM2000 specular reflector films, the light collection increases by 46%. This measured new light yield is used as an input to the simulation and the MDP decreases from 27.5% to 25% (see Figure 5).

4.2. Collimators

The original design of the PoGOLite Pathfinder includes active collimators made of plastic scintillators read out by a PMT after the scintillation light traverses the main plastic detector and a BGO scintillator (Figure 2). Since the plastic collimators are long and have a 2 mm wall, the loss of scintillation light for interactions happening far from the PMT results in a decrease in the detected signal amplitude. In general, for high amplitude signals, it is easy to distinguish in which component the interaction has taken place. This, however, becomes increasingly difficult for low energies. Tests performed on ground with a radioactive source illuminating only the collimator showed good performance above the trigger threshold (~ 20 keV)

²25 keV photon deposits ~ 1.2 keV when Compton scattering through 90° .

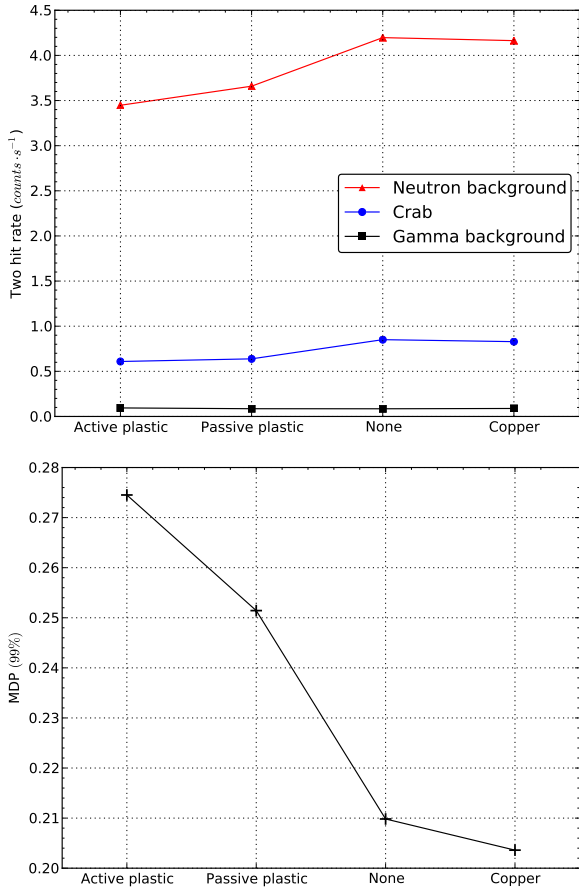


Figure 6: Polarimeter performance for four collimator types: “Active plastic” is the original active plastic collimators wrapped in $50\ \mu\text{m}$ thick lead and tin foils, “Passive plastic” is the same as the original but with passive plastic (not scintillating), “None” is with only the $50\ \mu\text{m}$ thick lead and tin foils and “Copper” is one with $0.5\ \text{mm}$ thick copper wrapped in $100\ \mu\text{m}$ thick lead and tin foils. The top figure displays the two-hit rate of the Crab (blue dots), the photon background (black squares) and the neutron background (red triangles) for each configuration. The bottom figure shows the corresponding performance in terms of MDP.

with 93% rejection efficiency but rather poor performance at lower energies (between the hit threshold $\sim 0.5\ \text{keV}$ and the trigger threshold) with 20% rejection efficiency [12]. In addition, as mentioned in Section 3, results from the 2013 flight showed waveform discrimination limitations when simultaneous interactions occur in the collimator and the detector of the same unit. In light of this, several passive collimators were studied to replace the original active collimators of the PoGOLite Pathfinder. Figure 6 shows the two-hit rate of the Crab, the neutron background and the photon background for four

configurations, as well as the corresponding performance in terms of MDP. The second configuration (“Passive plastic”) leads to a better MDP than the original active collimator (“Active plastic”) thanks to the improved reflective coating, which improves both the Crab two-hit rate (+4.8% relative) and the M_{100} (+7.0% relative). The first configuration does not benefit from the improved coating because active collimators need optical coupling to the detectors to be read-out by a single PMT (scintillation photons produced in the detector can escape to the collimator). The third configuration is a purely hypothetical scenario, where the collimator material itself has been removed but the protective lead and tin foils are still in place. The absence of the collimator material eliminates the shadowing of the underlying detectors, resulting in an increase in the exposed detector area (+36.6% relative) thus increasing the source rate. The M_{100} is also increased (+4.1% relative) for the same reasons as the second configuration. Although providing less shielding, the increase in source rate and M_{100} leads to a better MDP. However, this scenario is difficult to realise, as some supporting structure is needed for holding the lead and tin foils in place. In the fourth configuration, the copper collimators also increase the exposed detector area (+26.8% relative) and the M_{100} (+9.6% relative) compared to configuration 3 leading to a better MDP. The final configuration, with the active plastic collimator replaced by thin-walled copper collimators wrapped in lead and tin foils, will therefore be adopted for PoGO+, decreasing the MDP to 20.4%.

4.3. Detector length

Another way to improve the signal-to-background ratio is to optimize the size of the detectors. As the background is coming from every direction (proportional to the detector volume) whereas the source flux only comes from within the aperture (proportional to the detector area), having long detector rods enhances sensitivity to background. To study this effect, the length of the main plastic scintillator detectors has been decreased iteratively in Geant4, for the range 200 mm down to 50 mm. For each length, both Crab and background simulations are conducted. Figure 7 displays the results as a function of the detector length, both in terms of the resulting event rate and in terms of MDP. These results include the change in light collection

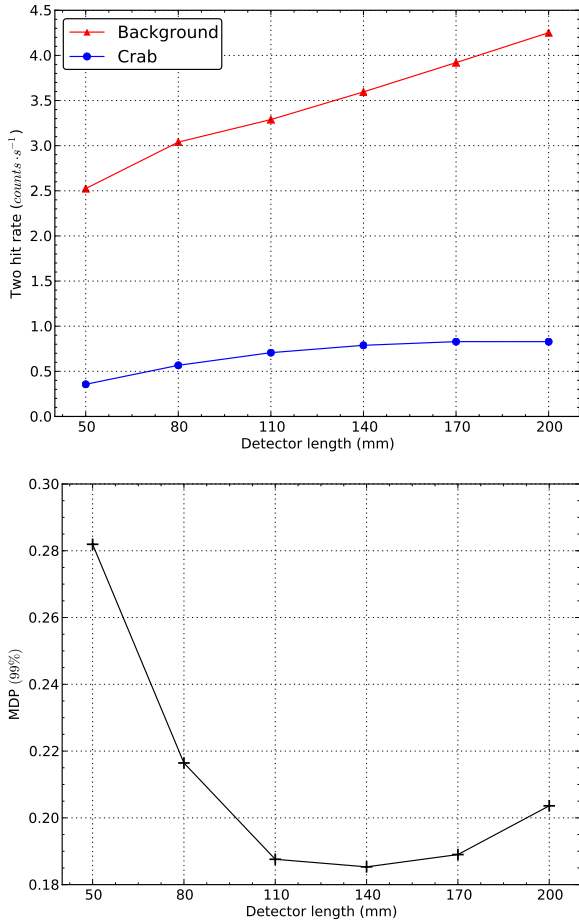


Figure 7: Polarimeter performance for varying detector lengths. The top plot shows the two-hit rate of the Crab (blue dots) and the background rate (red triangles) for each configuration, while the bottom figure shows the corresponding performance in terms of MDP.

interpolated from measurements, with a shorter detector resulting in higher light-collection than a longer one³. The background rate increases almost linearly with the detector length while the increase in the Crab rate saturates above 110 mm. A lower total rate will further decrease the MDP by increasing the live-time of the instrument⁴, therefore privileging shorter detectors. As the MDP is found to be stable between 120 mm and 140 mm, it has been decided that 120 mm long

³Comparative tests have been conducted with 10 cm and 20 cm long scintillator pieces, allowing a linear interpolation to be used.

⁴The live-time is not known at the moment since PoGO+ will use new electronics.

detectors will be adopted for PoGO+, providing better live-time as well as better light collection. The increase in performance resulting from this length optimisation is from 20.4% MDP to 18.6% MDP.

4.4. Neutron shield

The main source of background for PoGOLite is from neutrons produced in the atmosphere, as measured by the PoGOLino experiment [14] and by the neutron detector on board the PoGOLite Pathfinder [8]. This background is mitigated using a passive shield made of a hydrogen-rich material, i.e. polyethylene. The shield configuration used during the 2013 flight is shown in Figure 8-a. With a better understanding of the in-flight neutron environment, as well as a more complete simulation, it has been possible to re-optimize the shield geometry to further reduce the neutron background induced in the polarimeter. In particular, the region between the side and bottom neutron shield can be improved. Thus, three new designs have been studied in simulations. The shield geometries that have been considered are shown in Figure 8, while the corresponding MDP values are presented in Figure 9. Increased shield thickness

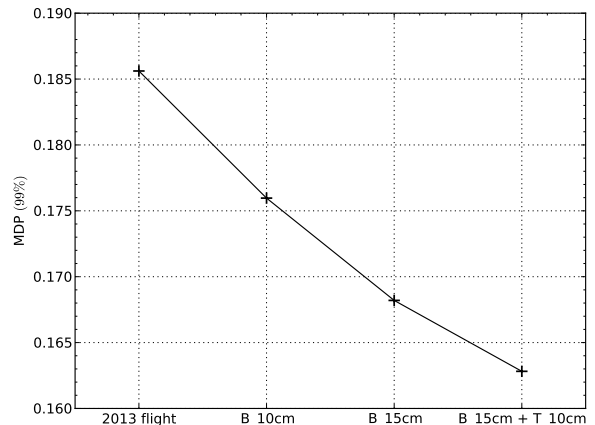


Figure 9: Polarimeter performance for different neutron shield configurations. Labels "2013 flight", "B_10 cm", "B_15 cm", and "B_15 cm + T_10 cm" correspond to Figure 8 a, b, c and d shield configurations, respectively.

improves the MDP, but the mass increases as well. Configurations (b), (c) and (d) add 16.8 kg, 51.5 kg and 100.7 kg, respectively, as compared to the 2013 flight geometry. The payload mass (~ 2 Tonnes) dictates the achievable flight altitude and thus the observation environment (source and background

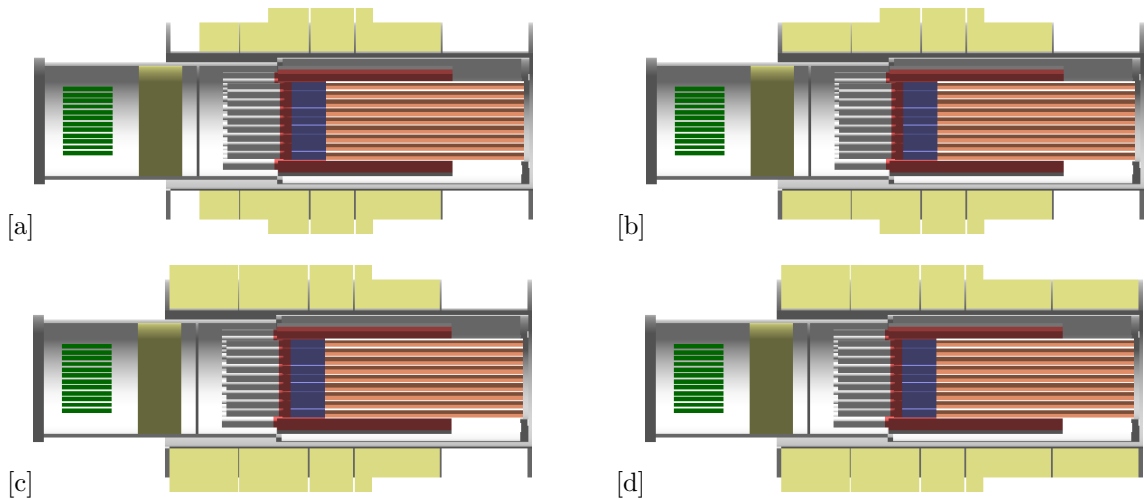


Figure 8: The different simulated shield configurations used for studying the neutron background. The PoGO+ Pathfinder original shield (a), one with additional 10 cm thick polyethylene at the bottom (b), one with all the bottom part thickness increased to 15 cm (c) and one with both 15 cm thick at the bottom and 10 cm thick at the top (d).

fluxes). As configuration (b) provides a good improvement with respect to the increase in mass⁵, this configuration has been chosen for the shield of PoGO+, resulting in an MDP of 17.6%.

5. PoGO+ expected performance

After the optimisation studies presented in the previous section, PoGO+ is currently under construction at KTH Royal Institute of Technology. The reflective coating and optical isolation of the detector cells have been reviewed, significantly increasing the light yield and M_{100} . The collimators have been changed from active plastic scintillators to thin-walled passive copper, reducing the shadowing of the detector area underneath the collimators and reducing both the induced background and complexity of the waveform discrimination veto. The length of the main plastic scintillator detectors has been shortened from 20 cm to 12 cm, reducing the volume for background interactions while not notably affecting efficiency for source detection. This shortening of the detectors also improves the light-yield and the observation live-time of the instrument by reducing the total event rate. The neutron shield will be upgraded by adding 10 cm thick polyethylene at the bottom of the instrument reducing the neutron rate by 12%. With this new design,

⁵It is assumed that the overall mass of the payload does not change.

PoGO+ is expected to reduce the MDP from 34.5% to 17.6% for a 6 hour Crab observation.

Calibration studies of the PoGO+ Pathfinder have shown that a strongly anisotropic flux coming from the side of the instrument can induce a fake polarisation signature [12]. It is therefore important to measure the background (off-source) to either show that no significant fake modulation is induced or for subtracting its modulation from the on-source measurement. When planning an in-flight observation, a suitable method for determining the fraction of time spent on-source and off-source is given by [15]:

$$\frac{T_{\text{off}}}{T_{\text{on}}} = \frac{1}{\sqrt{1 + R_S/R_B}}. \quad (3)$$

For instruments with modest signal-to-background ratio like PoGO+ ($R_S/R_B \sim 1/4$), $T_{\text{off}}/T_{\text{on}}$ approaches unity so PoGO+ will observe on-source and off-source for equal duration. Simulations with off-axis pointing scenarios show that the field of view is ~ 2 degrees, defined as twice the angle outside which the effective area drops below 50%. For an off-axis pointing of 5 degrees, the effective area is 0.07%, making this suitable for background measurements. Figure 10 shows the expected performance of PoGO+ assuming this 50% on-source observation strategy. The MDP for the Crab is calculated assuming an observation window of 6 hours per day, meaning 3 hours on-source and 3 hours off-source. The aforementioned MDP of 17.6% for 6

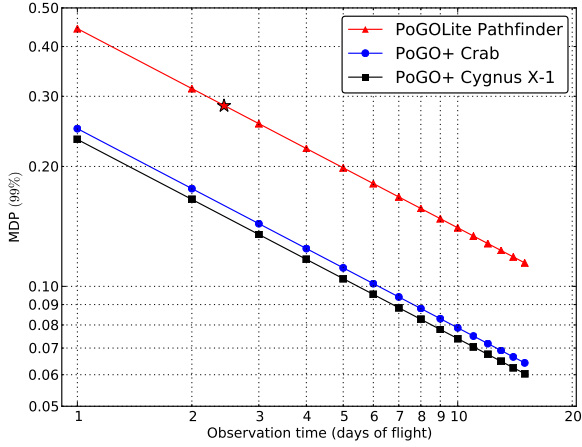


Figure 10: PoGO+ expected performance for the next flight assuming 50% time on-source (Crab or Cygnus X-1) and 50% time off-source (background fields). The MDP for the Crab (blue dots) and Cygnus X-1 (black squares) is shown as a function of the number of days of flight. For the Crab an observation window of 6 hours is assumed, for Cygnus X-1, 10 hours. The PoGOLite Pathfinder performance for the Crab (red triangles) is shown as a comparison and the red star shows the MDP for the Crab as observed during the 2013 flight [6].

hours of Crab observation is therefore achieved after a two-day flight. The MDP for Cygnus X-1 (black squares) is calculated assuming that the source is in the high state⁶ and an observation window of 10 hours per day (Cygnus X-1 is higher in the sky than the Crab as seen from Esrange during the Summer). Both the Crab and Cygnus X-1 are simulated using their respective average column density from the 2013 flight elevation and altitude profiles. Although the Crab emission rate is higher in the PoGO+ energy range, the difference in observation conditions leads to a better MDP for Cygnus X-1. The MDP of the PoGOLite Pathfinder design and 2013 flight for the Crab are also shown for comparison. The expected performance of PoGO+ for a 5 day flight reaches 11.1% MDP, while the corresponding number from the PoGOLite Pathfinder, extrapolated from the observed in-flight performance, would have been 19.8% MDP.

As an example of the quality of results that can be expected with such an increase in performance, a Crab observation with the reconstructed polarisation fraction and angle has been simulated us-

⁶A simple power law $2(E/\text{keV})^{-1.7}$ photons·cm⁻²·s⁻¹·keV⁻¹ is used to represent the hard state emission of Cygnus X-1 from 10 keV to 150 keV.

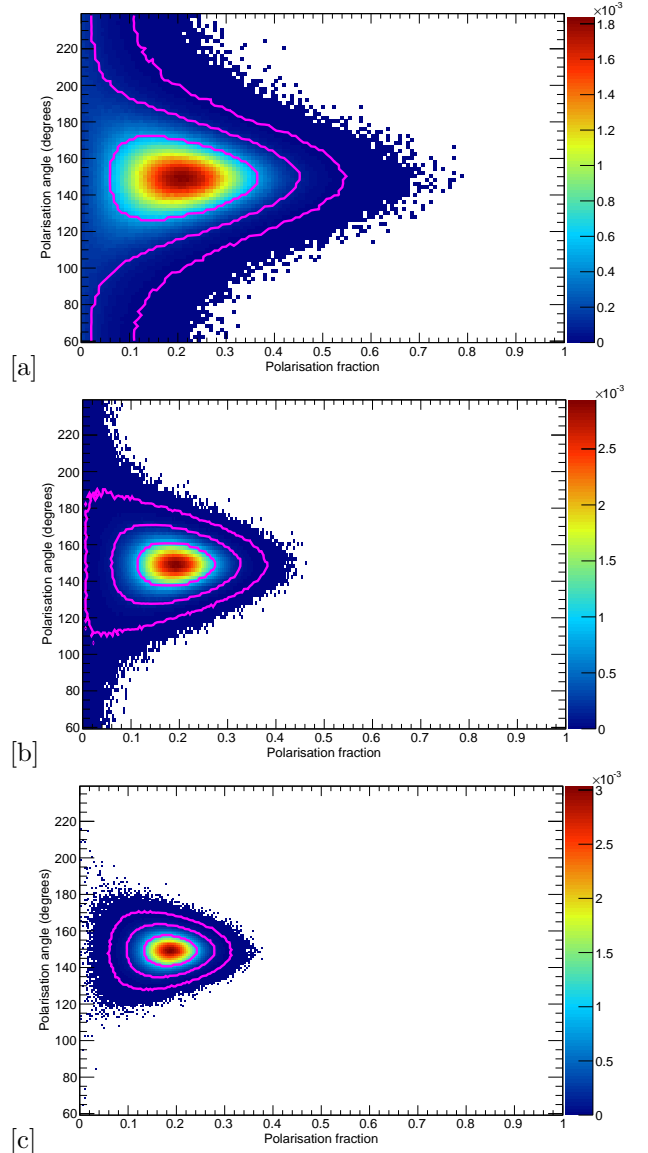


Figure 11: The posterior distribution of the polarisation fraction and polarisation angle of the Crab for: (a) the 2013 PoGOLite Pathfinder observations [6], (b) PoGO+ same 7.3 hour observation time and (c) PoGO+ 15 hours observation time. The two PoGO+ simulations assume the same central value of polarisation fraction and polarisation angle as (a). These results come from a Bayesian analysis method developed by [16]. The magenta lines are contours corresponding to 1, 2 and 3 standard deviations Gaussian probability content. The colour bar is the probability per bin.

ing a Bayesian analysis method [16]. This method uses the simulated M_{100} , Crab rate and background rate of PoGO+, as well as the expected polarisation fraction and polarisation angle as determined from the 2013 flight data, and produces a probabil-

ity map of the reconstructed polarisation fraction and polarisation angle. Figure 11 shows the results from the 2013 flight along with PoGO+ simulations for the same observation time as well as for a 5 day flight. While the PoGOLite Pathfinder measured a polarisation fraction of $(18.4^{+9.8}_{-10.6})\%$ [6], PoGO+ would measure a polarisation fraction 3.4 standard deviations from zero at $(18.4^{+5.32}_{-5.48})\%$ for the same observation time of 7.3 hours and 5.0 standard deviations from zero at $(18.4^{+3.72}_{-3.68})\%$ for a 5 day flight. In addition, PoGO+ will be sensitive enough to separate the contribution from the nebula through pulse phase selections. Such selections would reduce the source rate by 65.5% and the background rate by 60.0% but assuming a relatively high degree of polarisation from the nebula⁷ of 30%, PoGO+ would make a measurement of 4.5 sigma significance with a 5 day observation (prediction made with the same method as Figure 11). Phase-resolved polarimetry of the Crab has never been achieved in the energy range of PoGO+ and will provide new information on the emission geometry and mechanisms at work.

The studies presented here conservatively assume the same waveform discrimination efficiency as in the 2013 flight. It should be noted that this efficiency is expected to increase in the final design due to the removal of the active collimators, which simplifies the waveform discrimination process significantly. The MDP of PoGO+ for the Crab after a 5 day flight with a 100% waveform discrimination efficiency reaches 8.2%. The simulations also consider an average column density for the Crab and for Cygnus X-1 observations, which is also conservative as it results in higher than average absorption by the atmosphere leading to an overestimate of the MDP by $\sim 10\%$ (relative).

It is also foreseen to apply software improvements for the next flight, for example by only storing two-hit events, the live-time increases by $\sim 17\%$ directly affecting the polarimeter performance. Increasing the live-time will allow in-flight trigger thresholds to be relaxed, increasing the low-energy sensitivity of PoGO+, which is especially important due to the power-law behaviour of the source spectra.

⁷The polarisation fraction of the nebula is expected to be higher than the overall Crab emission [17].

6. Summary and Conclusions

The PoGOLite Pathfinder has made a successful flight in 2013, completing an almost full circumnavigation of the North Pole. As a proof-of-concept mission originally intended to validate the polarimeter design and pointing system, the flight also resulted in a polarisation measurement from the Crab with a polarisation fraction of $(18.4^{+9.8}_{-10.6})\%$. A thorough analysis of the flight data, the development of a detailed simulation, as well as a detailed and flight-validated background model have allowed the polarimeter design to be significantly improved in preparation for a re-flight. This upgraded design will improve the MDP by 44% (relative), reaching a value of 11.1% for the Crab and 10.5% for Cygnus X-1 (hard state) after a 5 day flight. Since these targets are visible at different times of the day, both can be studied in a single flight. Such performance will allow accurate polarisation measurement (5 standard deviation significance) of both sources in a previously unexplored energy range, 20 - 240 keV. PoGO+ will also allow the measurement of the Crab nebula polarisation fraction through pulse phase selections, giving unique insight into the location and mechanisms of emission. The new design is currently being implemented at KTH Royal Institute of Technology in Stockholm, Sweden. The reassembly of the polarimeter is expected to be finished during the second half of 2015, allowing calibration tests to begin before the end of the year, in preparation for a re-flight from Esrange, Sweden, in the Summer of 2016.

Acknowledgments

Funding received from The Swedish National Space Board, The Knut and Alice Wallenberg Foundation and The Swedish Research Council is gratefully acknowledged. KTH MSc students Håkan Wennlöf and Philip Ekfeldt are thanked for their contributions to laboratory studies. All past members of the PoGOLite Collaboration not listed as authors on this paper are thanked for their important contributions to the development of the project.

- [1] F. Lei, A. J. Dean, G. L. Hills, Compton Polarimetry in Gamma-Ray Astronomy, *Space Science Reviews* 82 (1997) 309–388. doi:10.1023/A:1005027107614.
- [2] H. Krawczynski, A. Garson, Q. Guo, M. G. Baring, P. Ghosh, M. Beilicke, K. Lee, Scientific prospects for hard X-ray polarimetry, *Astroparticle Physics* 34 (2011) 550–567. arXiv:1012.0321, doi:10.1016/j.astropartphys.2010.12.001.

- [3] M. C. Weisskopf, G. G. Cohen, H. L. Kestenbaum, K. S. Long, R. Novick, R. S. Wolff, Measurement of the X-ray polarization of the Crab Nebula, *The Astrophysical Journal, Letters* 208 (1976) L125–L128. doi:10.1086/182247.
- [4] M. Forot, P. Laurent, I. A. Grenier, C. Gouiffès, F. Lebrun, Polarization of the Crab Pulsar and Nebula as Observed by the INTEGRAL/IBIS Telescope, *The Astrophysical Journal, Letters* 688 (2008) L29–L32. arXiv:0809.1292, doi:10.1086/593974.
- [5] A. J. Dean, D. J. Clark, J. B. Stephen, V. A. McBride, L. Bassani, A. Bazzano, A. J. Bird, A. B. Hill, S. E. Shaw, P. Ubertini, Polarized Gamma-Ray Emission from the Crab, *Science* 321 (2008) 1183–. doi:10.1126/science.1149056.
- [6] M. Chauvin, H.-G. Florén, M. Jackson, T. Kamae, T. Kawano, M. Kiss, M. Kole, V. Mikhalev, E. Moretti, G. Olofsson, S. Rydström, H. Takahashi, A. Iyudin, M. Arimoto, Y. Fukazawa, J. Kataoka, N. Kawai, T. Mizuno, F. Ryde, H. Tajima, T. Takahashi, M. Pearce, Observation of polarised hard X-ray emission from the Crab by the PoGOLite Pathfinder, ArXiv e-prints, accepted in MNRAS Letters arXiv:1511.02735.
- [7] M. C. Weisskopf, R. F. Elsner, S. L. O’Dell, On understanding the figures of merit for detection and measurement of X-ray polarization, in: Society of Photo-Optical Instrumentation Engineers (SPIE) Conference Series, Vol. 7732 of Society of Photo-Optical Instrumentation Engineers (SPIE) Conference Series, 2010, p. 0. arXiv:1006.3711, doi:10.1117/12.857357.
- [8] M. Chauvin, H.-G. Florén, M. Jackson, T. Kamae, T. Kawano, M. Kiss, M. Kole, V. Mikhalev, E. Moretti, G. Olofsson, S. Rydström, H. Takahashi, J. Lind, J.-E. Strömberg, O. Welin, A. Iyudin, D. Shifrin, M. Pearce, The design and flight performance of the PoGOLite Pathfinder balloon-borne hard X-ray polarimeter, *Experimental Astronomy* arXiv:1508.03345, doi:10.1007/s10686-015-9474-x.
- [9] S. Agostinelli, J. Allison, K. Amako, J. Apostolakis, H. Araujo, P. Arce, M. Asai, D. Axen, S. Banerjee, G. Barrand, F. Behner, L. Bellagamba, J. Boudreau, L. Broglia, A. Brunengo, H. Burkhardt, S. Chauvie, J. Chuma, R. Chytráček, G. Cooperman, S. Cosmo, P. Degtyarenko, A. Dell’Acqua, G. Depaola, D. Dietrich, R. Enami, A. Feliciello, C. Ferguson, H. Fesefeldt, G. Folger, F. Foppiano, A. Forti, S. Garelli, S. Giani, R. Giannitrapani, D. Gibin, J. J. Gómez Cadenas, I. González, G. Gracia Abril, G. Greeniaus, W. Greiner, V. Grichine, A. Grossheim, S. Guatelli, P. Gumplinger, R. Hamatsu, K. Hashimoto, H. Hasui, A. Heikkinen, A. Howard, V. Ivanchenko, A. Johnson, F. W. Jones, J. Kallenbach, N. Kanaya, M. Kawabata, Y. Kawabata, M. Kawaguti, S. Kelner, P. Kent, A. Kimura, T. Kodama, R. Kokoulin, M. Kossov, H. Kurashige, E. Lamanna, T. Lampén, V. Lara, V. Lefebure, F. Lei, M. Liendl, W. Lockman, F. Longo, S. Magni, M. Maire, E. Medernach, K. Minamimoto, P. Mora de Freitas, Y. Morita, K. Murakami, M. Nagamatu, R. Nartallo, P. Nieminen, T. Nishimura, K. Ohtsubo, M. Okamura, S. O’Neale, Y. Oohata, K. Paech, J. Perl, A. Pfeiffer, M. G. Pia, F. Ranjard, A. Rybin, S. Sadilov, E. Di Salvo, G. Santin, T. Sasaki, N. Savvas, Y. Sawada, S. Scherer, S. Sei, V. Sirotenko, D. Smith, N. Starkov, H. Stoecker, J. Sulkimo, M. Takahata, S. Tanaka, E. Tcherniaev, E. Safai Tehrani, M. Tropeano, P. Truscott, H. Uno, L. Urban, P. Urban, M. Verderi, A. Walkden, W. Wander, H. Weber, J. P. Wellisch, T. Wenaus, D. C. Williams, D. Wright, T. Yamada, H. Yoshida, D. Zschiesche, GEANT4 Collaboration, GEANT4—a simulation toolkit, *Nuclear Instruments and Methods in Physics Research A* 506 (2003) 250–303. doi:10.1016/S0168-9002(03)01368-8.
- [10] R. Brun, F. Rademakers, ROOT — An object oriented data analysis framework, *Nuclear Instruments and Methods in Physics Research A* 389 (1997) 81–86. doi:10.1016/S0168-9002(97)00048-x.
- [11] T. Mizuno, Y. Kanai, J. Kataoka, M. Kiss, K. Kurita, M. Pearce, H. Tajima, H. Takahashi, T. Tanaka, M. Ueno, Y. Umeki, H. Yoshida, M. Arimoto, M. Axelsson, C. Marini Bettolo, G. Bogaert, P. Chen, W. Craig, Y. Fukazawa, S. Gunji, T. Kamae, J. Katsuta, N. Kawai, S. Kishimoto, W. Klamra, S. Larsson, G. Madejski, J. S. T. Ng, F. Ryde, S. Rydström, T. Takahashi, T. S. Thurston, G. Varner, A Monte Carlo method for calculating the energy response of plastic scintillators to polarized photons below 100 keV, *Nuclear Instruments and Methods in Physics Research A* 600 (2009) 609–617. doi:10.1016/j.nima.2008.11.148.
- [12] M. Chauvin, M. Jackson, T. Kawano, M. Kiss, M. Kole, V. Mikhalev, E. Moretti, H. Takahashi, M. Pearce, Preflight performance studies of the PoGOLite hard X-ray polarimeter, *Astroparticle Physics* 72 (2016) 1–10. arXiv:1505.08093, doi:10.1016/j.astropartphys.2015.05.003.
- [13] M. Kole, M. Pearce, M. Muñoz Salinas, A model of the cosmic ray induced atmospheric neutron environment, *Astroparticle Physics* 62 (2015) 230–240. arXiv:1410.1364, doi:10.1016/j.astropartphys.2014.10.002.
- [14] M. Kole, M. Chauvin, Y. Fukazawa, K. Fukuda, S. Ishizu, M. Jackson, T. Kamae, N. Kawaguchi, T. Kawano, M. Kiss, E. Moretti, M. Pearce, S. Rydström, H. Takahashi, T. Yanagida, PoGOLino: A scintillator-based balloon-borne neutron detector, *Nuclear Instruments and Methods in Physics Research A* 770 (2015) 68–75. arXiv:1410.2377, doi:10.1016/j.nima.2014.10.016.
- [15] F. Kislat, B. Clark, M. Beilicke, H. Krawczynski, Analyzing the data from X-ray polarimeters with Stokes parameters, *Astroparticle Physics* 68 (2015) 45–51. arXiv:1409.6214, doi:10.1016/j.astropartphys.2015.02.007.
- [16] V. Mikhalev, A&A, in preparation.
- [17] J. Dyks, A. K. Harding, B. Rudak, Relativistic Effects and Polarization in Three High-Energy Pulsar Models, *The Astrophysical Journal* 606 (2004) 1125–1142. arXiv:astro-ph/0401255, doi:10.1086/383121.